JOURNAL OF MATERIALS SCIENCE 25 (1990) 2990–2996

Dependence of high-temperature tensile strength on displacement rate for hot-pressed silicon nitride

TATSUKI OHJI, YUKIHIKO YAMAUCHI, WATARU KANEMATSU, SHOJI ITO
Government Industrial Research Institute, Hirate-cho, Kita-ku, Nagoya 462, Japan

Tensile tests of hot-pressed silicon nitride were conducted in a wide range of displacement rates from 0.0005 to 50.0 mm min^{-1} at 1260 and 1380° C, and the dependence of strength on displacement rate was discussed in conjunction with the change of fracture surface features. As displacement rate was lowered, strength was degraded and stress-displacement diagrams altered from linearity to non-linearity, accompanying appearances of yielding phenomena. Strength was largely dependent on displacement rate in the high-rate region and rather independent in the low-rate region. The fracture surface features were drastically changed from brittle fracture to subcritical crack-growth fracture with decreasing displacement rate. A further increase in stress following the lower yielding point in the low-rate region was attributed to increments of fracture resistance due to the pull-out contribution of elongated grains.

1. Introduction

Silicon nitride has been considered one of the most promising ceramic materials as a candidate for high temperature structural components. Generally, however, the mechanical strength is degraded at high temperatures owing to the reduction in viscosity of amorphous phases formed at grain boundaries caused by processing with sintering additives. In the past ten years efforts have been made to minimize the number of amorphous phases or to crystallize them, resulting in materials with excellent strength properties at high temperatures above 1200° C [1]. For instance, however, pressureless sintered materials, which possess remarkable superiority over hot-pressed materials regarding near-net-shape fabrication, are usually doped with a considerable amount of oxides, and as a result still include some glassy phase at their grain boundaries [2].

In the temperature range where the glassy phases are softened, grain boundaries show visco-elastic behaviour, and subcritical crack growth (SCG) propagating through them is the predominant factor in determining strength properties, particularly in the strength related to delayed fractures like creep strength [3, 4]. Also in this region, due to the pull-out contribution of elongated grains to crack-propagation resistance or crack blunting induced by grain boundary sliding, fracture toughness is apparently increased in some measurements, though strength is decreased [5–10]. Therefore, a better understanding of the crack propagation process and its correlation with strength properties in this range is very important not only from the viewpoint of mechanical property assessment and practical applications, but also with respect to the effectiveness of pull-out toughening mechanisms such as whisker reinforcement.

In the above region, as the failure process is associated with grain boundary sliding, cavity nucleation and propagation, enhanced grain pull-out contribution, etc., the stress–displacement (S–D) relationships in mechanical strength tests exhibit non-elastic characteristics. In order to obtain information on the failure properties of materials which exhibit non-elastic deformation, uniaxial tensile testing is recognized as the best method because the specimen is subjected to uniform stress so that measured results can be analysed precisely and simply. Thus many approaches have been conducted towards the accurate tensile testing of ceramics [11–13].

In previous works [14, 15], non-elastic behaviour at elevated temperatures in S–D diagrams of tensile tests were investigated for several kinds of silicon nitride. In this study, tensile tests of hot-pressed silicon nitride were conducted in the extended region of displacement rates at 1260 and 1380° C, and the dependence of strength on strain rates, especially in extremely high- and low-rate regions, and the fractographic features were discussed in association with crack nucleation and propagation processes.

2. Experimental procedures

Commercially available hot-pressed silicon nitride doped with 5 wt % yttria and 3 wt % alumina containing impurities of 0.012% magnesium, 0.013% chromium, 0.022% iron and 0.024% calcium, (wt %) was used in this study. The density was determined to be 3.199 Mg m^{-3} by water immersion. Tensile test specimens, which are plate-like (Fig. 1) were fabricated from billets of hot-pressed silicon nitride in a profile grinding machine so that the longitudinal direction of the specimen is perpendicular to the hot-pressing direction. The gauge length area of specimens was

0022–2461/90 $03.00 + .12

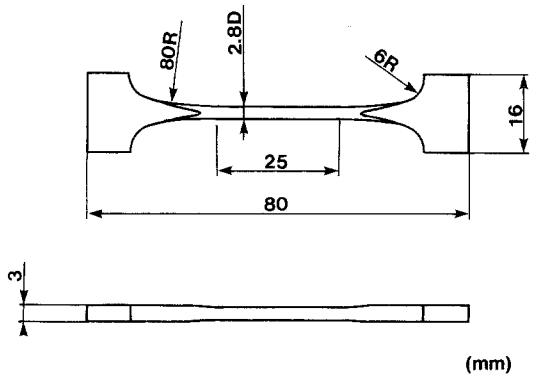

Figure 1 Geometry and dimensions of tensile test specimen.

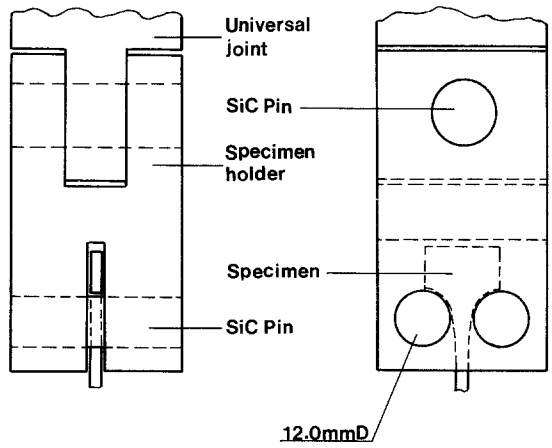

Figure 2 Tensile testing apparatus for low displacement-rate measurements.

hand polished along its length with 2000-grid diamond paste to eliminate surface flaws introduced in machining process.

The tensile testing equipment is shown in Fig. 2. For the low displacement rate measurements, silicon carbide pins to hold specimens were made so that they exactly conformed to a specimen's shoulder, to prevent local deformation at the support portion. The specimen holders were connected into pulling rods through the universal joints. Using four strain gauges attached into central parts of the gauge length area, axial alignment was ensured for each test with loading up to 500 N so that the bending stress on the surface was suppressed to within 4% of the tensile stress before raising temperature. During heating, a load of 5 N was constantly applied so as not to disturb the axial alignment by heat expansion. Tests were conducted in a vacuum atmosphere of 10^{-4} torr at room temperature and above (1260 and 1380° C). The furnace reached test temperatures in about 30 min, and the specimen was held for 30 min at these temperatures before tests were begun, to achieve thermal equilibrium. The uniformity of temperature along the gauge length area of specimens was verified to be within 3° C using a PtRh6-30 thermocouple. Crosshead speed was varied from 0.0005 to 50.0 mm min^{-1}, which was the limit for relaible measurements of the employed load cells. Three specimens were used for each measurement.

3. Results and discussion

3.1. Change of S–D diagrams with displacement rate

The non-elastic behaviour of hot-pressed silicon nitride at 1300 to 1400° C has been described previously [14]. Summarized briefly, strength is maintained at around 700 MPa up to 1000° C but drastically degraded above this temperature when the displacement rate (crosshead speed) is fixed at 0.1 mm min^{-1}. At 1260° C, S–D diagrams of tensile tests begin to show some non-elasticity, and at 1300° C stress falls showing a peak (upper yielding point) before fracture. Above 1340° C, stress is re-increased through a transitional point (lower yielding point) after the peak, and describes large curvature up to the final fracture strength (ultimate strength). These phenomena are also greatly affected by displacement rates, but the ultimate strength tends to depend on temperature rather than displacement rate. The first stress peak, upper yielding point, is attributed to the rapid expansion of the cavitation zone accompanied by grain-boundary sliding [16, 17] and the stress re-increase (ultimate strength) is due to increments of crack propagation resistance caused by the morphology of silicon nitride grains [5].

In this paper, emphasis is placed on investigations of the displacement rate dependence of strength or S–D relationship, in the wide-rate range. The results at 1260° C are shown in Fig. 3a and b, where the stress is the load divided by the original cross-sectional area of the specimen, or the engineering stress. The displacements shown in the figures are the distance moved by the cross-head of the testing device, which includes elongations of the apparatus itself and the tapered portion of the specimen. Similar experiments using an electro-optical extensometer in air revealed that the real elongation of gauge length was almost always about 70% of the displacement of the cross head, and most of the rest is due to elongation of the tapered portion of the specimen [18]. As the displacement rate rose from 0.1 mm min^{-1}, the elasticity was expanded until fracture in the S–D diagrams with increasing fracture stress, and a strength higher than 500 MPa was attained in the rate region above 10.0 mm min^{-1}. On lowering of the displacement rate, the peak of stress (upper yielding point) presents itself, and in the region lower than 0.002 mm min^{-1}, a gradual stress re-increase accompanied with large elongations was observed after yielding points. These curves tend to converge into a certain value, ultimate strength, which is almost irrespective of displacement rates, while yielding points are seriously affected by them.

The results obtained at 1380° C are shown in Fig. 4. At 1380° C, even the rate of 50 mm min^{-1} gave small deviation from linearity immediately before fracture. Although strength ranged widely with changing displacement rate, below 0.5 mm min^{-1} the stress re-increase behaviour after the lower yielding point, ultimate strength, played the role of determining each strength, leading to a rather stable value as with 1260° C. In fractures below 0.005 mm min^{-1}, no upper and lower yielding points were observed. The specimen failed at 0.001 mm min^{-1} showed about 1.2 mm elongation after the temperature was cooled. This is nearly equal to the elongation measured by the above

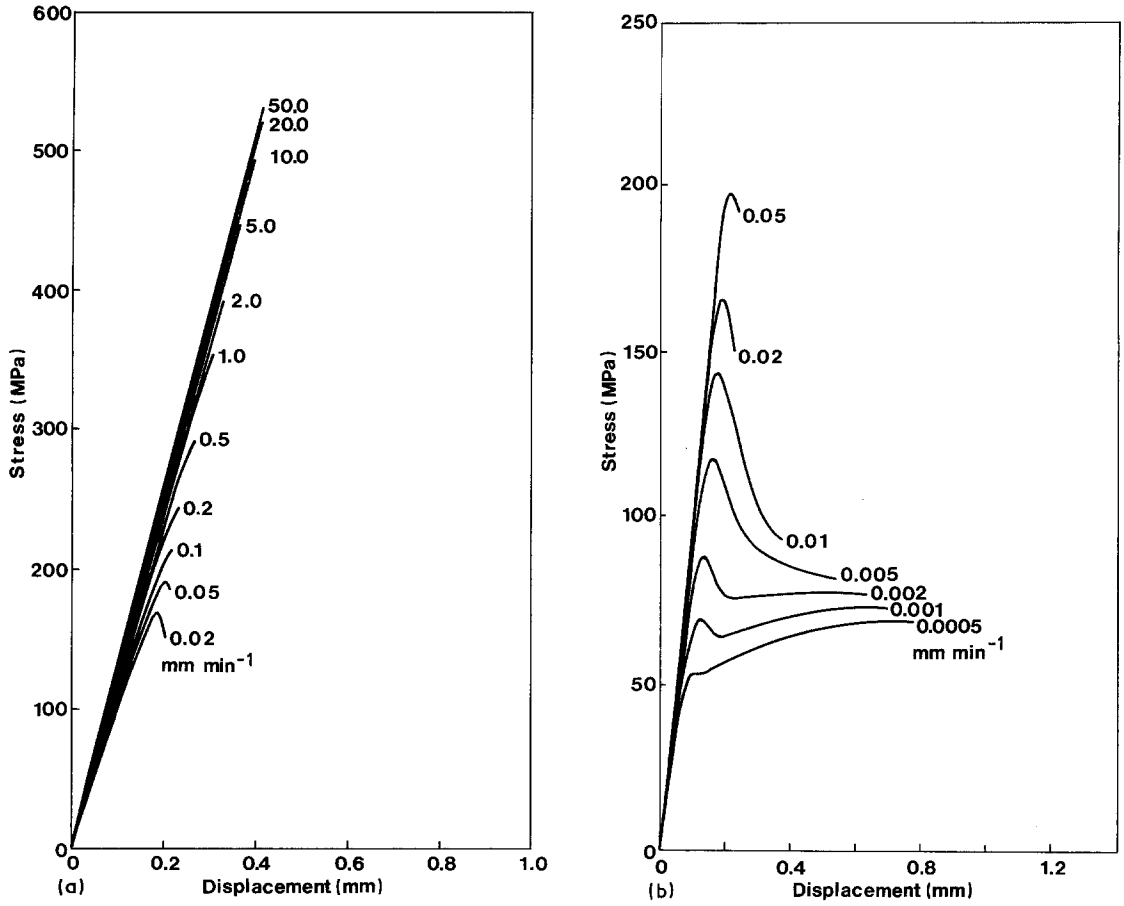

Figure 3 Stress–displacement diagrams of hot-pressed silicon nitride as a function of displacement rate. (a) High rate region; (b) low rate region. Temperature, 1260° C.

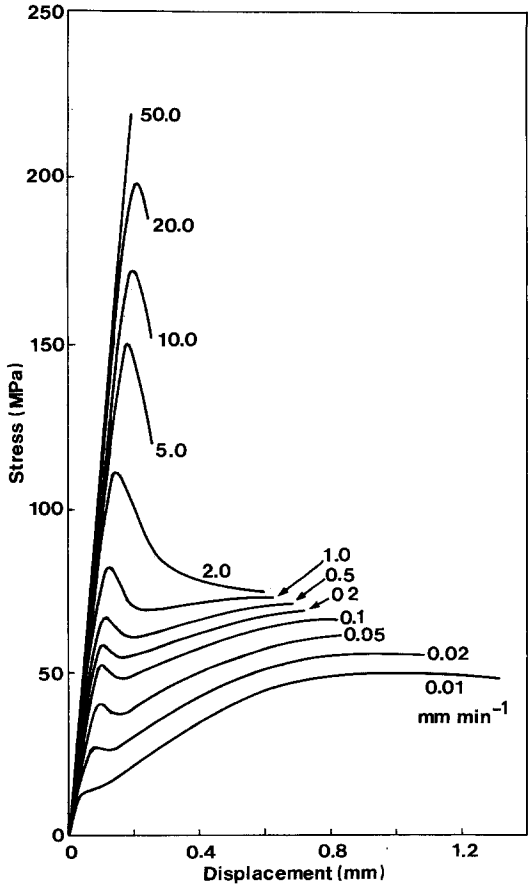

Figure 4 Stress–displacement diagrams of hot-pressed silicon nitride as a function of displacement rate. Temperature, 1380° C.

electro–optical extensometer under air atmosphere at the same temperature and displacement rate [18].

As described above, the upper yielding point is assumed to be caused by the rapid spread of the cavitation zone. This zone spreading requires a sufficient initial cavity growth at the grain boundary [16, 17]: namely, initial cavity growth induces irregular stress distribution and accelerates cavitation expansion. Evans *et al.* [16] characterized cavity growth along grain boundaries in traction material containing a continuous glassy phase around the grains as follows

$$t_p\dot{\varepsilon}_\infty = \lambda(b/\delta_0)^2 \quad (1)$$

where t_p is the time to create a facet sized cavity, $\dot{\varepsilon}_\infty$ is the remote strain rate, b is the distance between cavities, δ_0 is the initial thickness of the amorphous phase, and λ is a coefficient primarily depending on the grain size and viscosity of the glassy phase. Although the rapid cavitation zone expansion occurs while the cavity is still small, and hence does not require a facet-sized cavity, the time to form the initial cavity, t_c, is characterized in a similar manner. The term $(b/\delta_0)^2$ is regarded as a material constant at a certain temperature. If the zone spreading occurs, the moment the initial cavity is formed, $\dot{\varepsilon}_\infty$ and t_c in Equation 1 can be replaced by the displacement rate, $\dot{D}$, and the time up to upper yielding point, t_u as follows

$$D_u = t_u\dot{D} = \text{const.} \quad (2)$$

where D_u is the displacement up to upper yielding

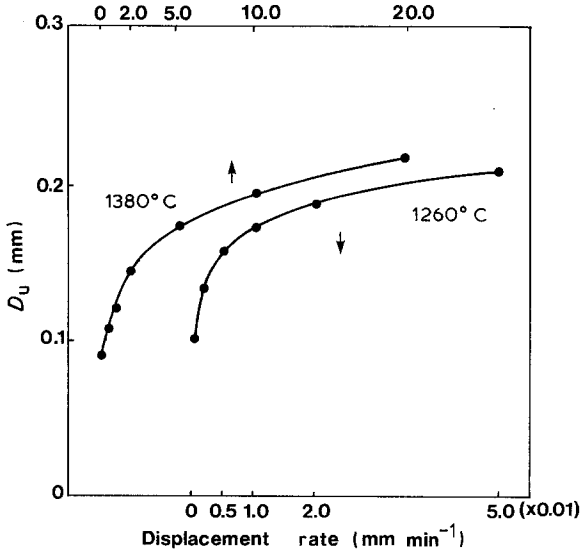

Figure 5 Dependences of displacement up to upper yielding point, D_u, on displacement rate at 1260 and 1380° C.

point. Namely, t_u is not proportional to the displacement rate. In Fig. 5, D_u is plotted against displacement rate. In fact, it is assumed to take the time t_s to spread the cavitation zone after initial cavity is formed, and hence D_u is given by

$$D_u = (t_u + t_s)\dot{D} = C + t_s\dot{D} \qquad (3)$$

where C is a constant. D_u ranges from 0.1 to 0.2 and increases with increasing displacement rate, the slope getting lower at both temperatures. This means t_s is a function of the displacement rate, and high in the low-rate region and low in the high-rate region, while t_u is very roughly unproportional against displacement rate.

3.2. Displacement rate dependence of strength

In Fig. 6, the dependences of strength on displacement rate at room temperature, 1260 and 1380° C are exhibited in semi-log form as Trantina [19] suggests the exponential crack growth formulation was more suitable for the interpretation of high-temperature strength degradation of hot-pressed silicon nitride than the power-law formulation. Also in this study, when adopting the log–log form, clear changes in displacement-rate dependence of high-temperature strength, as shown in Fig. 6, were not obtained.

Measurement at room temperature was also conducted in a vacuum atmosphere to prevent SCG due to stress corrosion [20]. It is known that at room temperature there is almost no displacement-rate dependence of strength. At 1260° C, the displacement-rate dependence of strength is divided into three regions: above 0.5 mm min^{-1}, between 0.5 and 0.001 mm min^{-1}, and below 0.001 mm min^{-1}. In the respective regions, fracture strength is determined by failure stress with elasticity or little plasticity, upper yielding point and ultimate strength, though in the region between 1.0 and 0.1 mm min^{-1} it is difficult to know whether failure is fracture with placticity, or the upper yielding phenomenon from the S–D diagrams. Likewise, at 1380° C, similar changes occur around 20.0 and 0.5 mm min^{-1}, respectively.

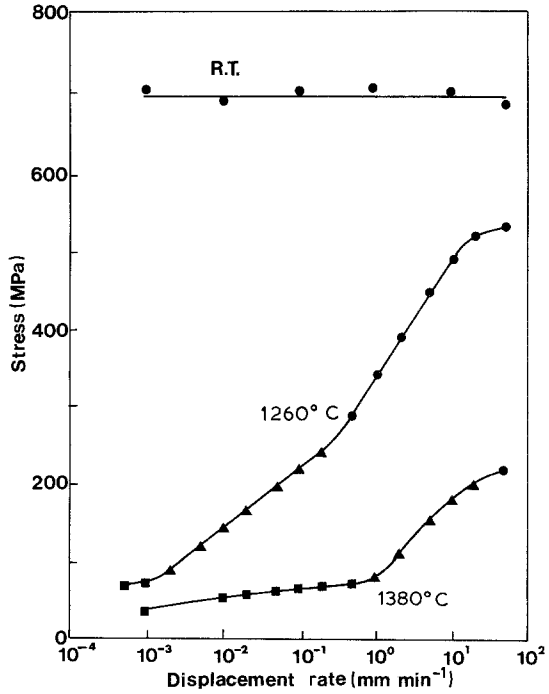

Figure 6 Dependences of strength on displacement rate at room temperature, 1260 and 1380° C. Data are plotted by the mean value of three specimens. Failure stress with ●, elasticity or little plasticity; ▲, upper yielding point; ■, ultimate strength.

It is worthy of note that strength tends to be saturated as displacement rate is raised up to 50 mm min^{-1}, suggesting the presence of fast-fracture strength peculiar to the material and temperature which is independent of the displacement rate. This result is consistent with the fact that impact strength is degraded at temperatures higher than 1200° C for several kinds of silicon nitride doped with alumina and yttria [21]. Consequently, the rate dependence of high-temperature strength consists of four regions: two rather stable regions in the extremely high- or low-rate regions, and two sensitive regions in the medium-rate region. It should be pointed out that many standards for flexure tests of ceramic materials provide the cross-head speed corresponding to stressing rate in this medium region [22, 23].

3.3. Fracture surface topography

At high temperatures where silicon nitride showed strength degradation, fractographic features were greatly variable with the change of displacement rate [24]. Figure 7 shows fracture surfaces of hot-pressed silicon nitride tensile specimens at 1260 and 1380° C. The specimen failed at 50 mm min^{-1} showed the typical fracture surface of brittle materials, comprising smooth and rough areas which are usually referred to as fracture mirror and hackle or macroscopic crack branching, respectively [25], and, therefore, it is very similar to that fractured at room temperature [3, 26]. This fact also agrees with the linear S–D diagram in Fig. 3. In the fracture of 1.0 mm min^{-1}, a smooth area was largely expanded so that a small rough area was left at the circumference. However, the wake of SCG cannot be seen in SEM observations, although the S–D diagram offers a small deviation from linearity in the vicinity of the fracture point. Fracture

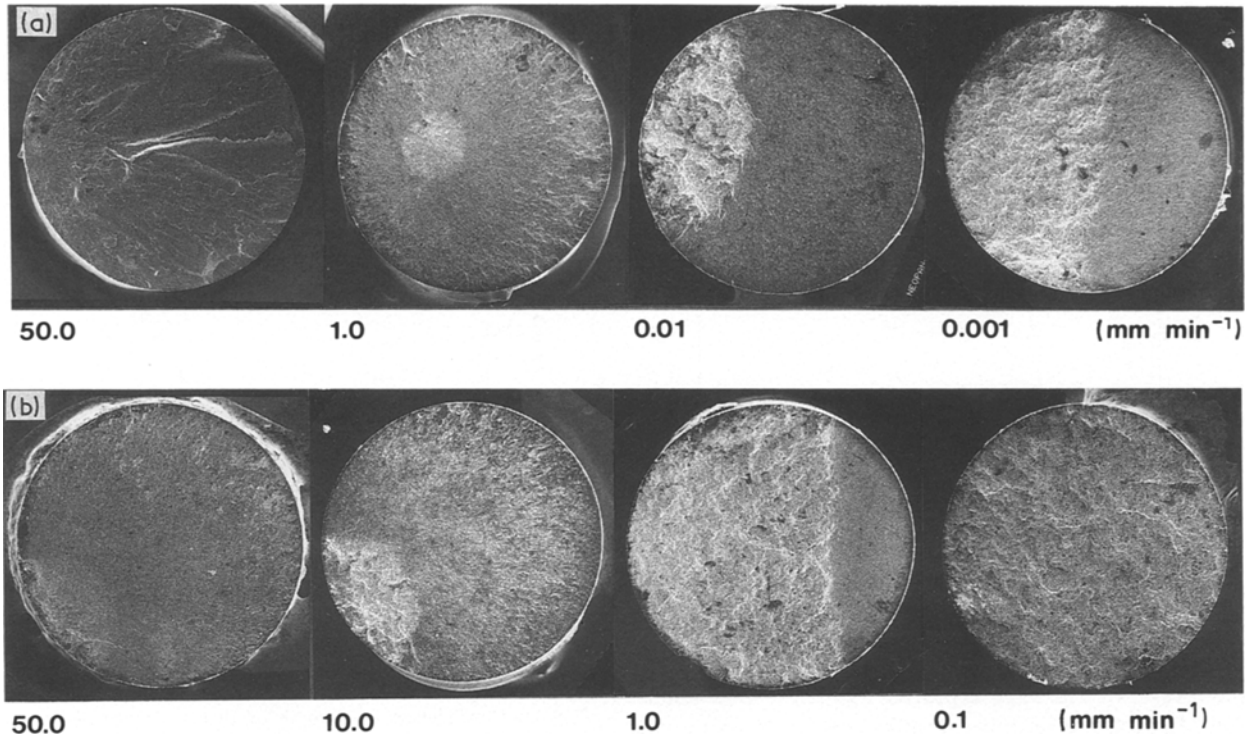

Figure 7 Change of fracture surface features with displacement rate at (a) 1260 and (b) 1380° C. Diameter, 2.8 mm.

surfaces of 0.01 and 0.001 mm min^{-1} were composed of a smooth area and another rough area (SCG area). The SCG area was expanded as displacement rate decreased down to 0.002 mm min^{-1}. Below this rate, as final strengths were converged, SCG areas remained unchanged and constantly formed half of all areas, as shown in the top right of Fig. 7 (0.001 mm min^{-1}).

In the case of 1380° C, at 50 mm min^{-1} a narrow SCG area was observed at the edge of surface, reflecting a slight non-linearity immediately before fracture. It is known that fractures of 50.0 and 10 mm min^{-1} at 1380° C existed between 1.0 and 0.001 mm min^{-1} at 1260° C in terms both of strength and fracture surface. The SCG area was expanded with lowering of the displacement rate, and in fractures at 0.1 mm min^{-1} and lower, the SCG area covered almost the full area of the fracture surface. Although the ultimate strength at these rates is nearly equal to that of 0.002 to 0.0005 mm min^{-1} at 1260° C, as mentioned before, the ratio of the SCG area over the total sectional area is largely different in fracture surfaces. This fact suggests that the fracture toughness was apparently increased at 1380° C. This is probably due to the fact that as temperature rises, the grain boundary strength is lowered owing to the softening of glassy phase, resulting in visco-elastic pulling-out of elongated grains as well as easy growth of cracks. Consequently, the final fracture requires a larger crack than is the case at 1260° C.

3.4. Crack propagation mechanism

Fracture surfaces sometimes consist of smooth and rough (SCG) areas as in the top right of Fig. 7 (0.001 mm min^{-1}). In this fracture surface, the wakes of crack growth were investigated by SEM observation. Figs. 8a and b show SEM images taken from rough and smooth areas of that surface, respectively. It is recognized that the wakes of the crack propagation in smooth and rough areas are very similar. The difference between them is that the surface of Fig. 8b is on the whole rather even than (a), and (b) has fewer holes or protruding grains than (a). The same feature as in

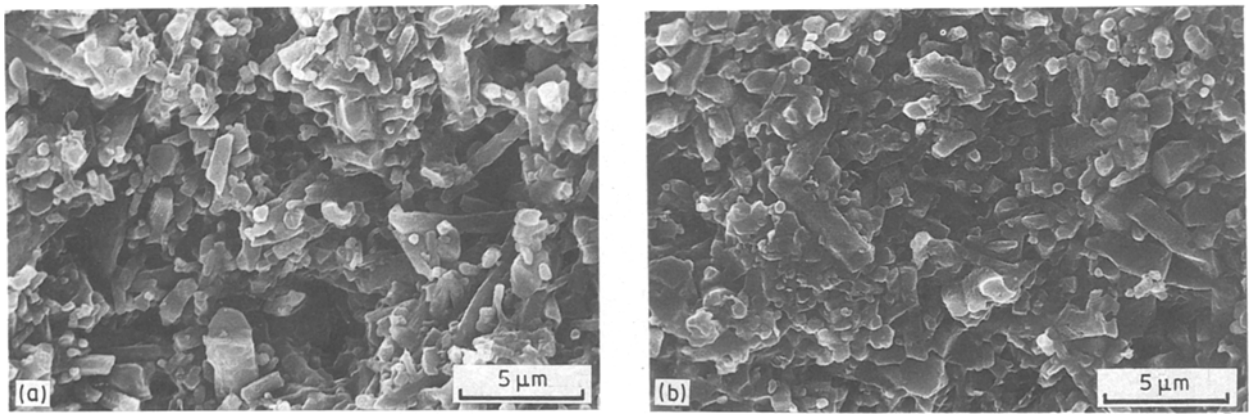

Figure 8 Microstructures of crack propagation wakes in fracture of 0.001 mm min^{-1} at 1260° C. (a) Rough area; (b) smooth area.

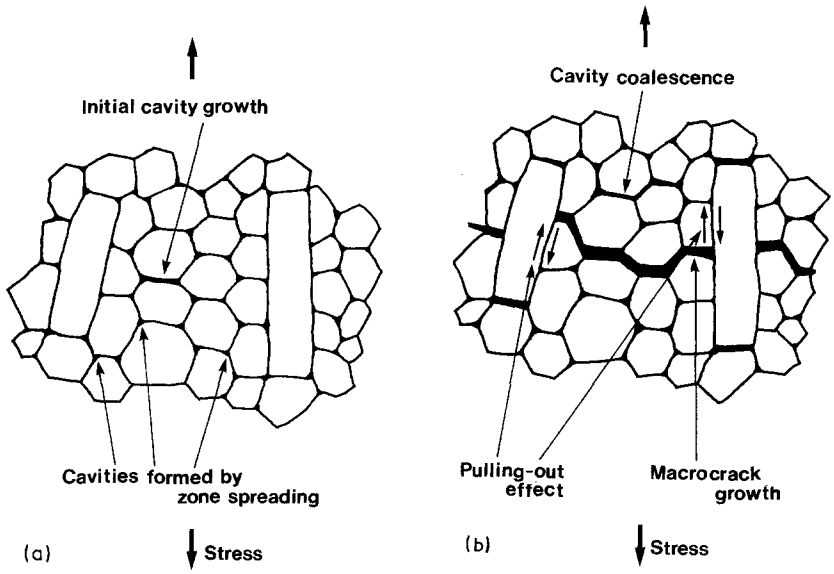

Figure 9 Schematic drawing of cavity formation and crack propagation. (a) Initial cavity growth and cavitation zone spreading; (b) cavity coalescence and macrocrack propagation with pulling out of elongated grains.

(b) was observed in a whitish area around the fracture point of 0.1 mm min^{-1} in Fig. 7.

Figure 9 schematically represents the cavitation zone spreading (a) and the major crack propagation (b). In this figure several equiaxed grains, presumably elongating in the perpendicular direction to the plane are assumed to be put between two elongated grains. A similar feature of morphology is sometimes observed in silicon nitride [6, 27, 28]. As the upper yielding point is attributed to the rapid expansion of the cavitation zone, cavities are supposed to be distributed into many triple points (or grain boundaries) throughout specimens as shown in Fig. 9a, when the applied stress reaches the upper yielding point in the diagram of 0.001 mm min^{-1} in Fig. 3. These cavities play a major part in inducing crack nucleation and propagation. After the upper yielding point, a microcrack originating from the cavity at triple point was extended along the boundary and, when these microcracks were connected with each other, cavity coalescence was induced resulting in the initiation of SCG. In the area where SCG was expanding, the elongated grains were gradually being pulled out (Fig. 9a). This pulling out produces further fracture resistance, leading to a stress re-increase in the S–D diagram. Consequently, many holes and protruding grains were left in the wake of SCG after fracture (Fig. 8a). When SCG is expanded to the critical size, cracks propagate catastrophically in the remaining area. However, as the zone spreading and formation of cavity coalescences should also be extended to this area, rapid crack propagation is strongly associated with these cavities or microcracks. Hence most of the microstructure in the smooth area also shows clear grain boundaries, but few holes and protruding grains remain (Fig. 9b).

This tendency is true in every surface where the wake of SCG is observed in fracture surfaces; the rough (SCG) area includes many holes and protruding grains, and the smooth has only a few, while both are primarily intergranular fractures. The case of 0.1 mm min^{-1} at 1260° C, which showed small plasticity in the S–D diagram, owed its similar microstructure to the smooth area around the fracture initiation site in the fracture surface, but no wake of SCG. Just before the fracture, the zone spreading and cavity coalescence are supposed to have occurred, but the applied stress was too high to bear SCG and clear pulling-out of grains.

4. Conclusions

Tensile tests of hot-pressed silicon nitride were conducted in a wide region of displacement rates from 0.0005 to 50.0 mm min^{-1} at 1260 and 1380° C, and the dependence of strength on displacement rate was investigated in conjunction with the change of fractographic features. As displacement rate was changed from high to low, strength was degraded and S–D diagrams altered from linearity to non-linearity accompanying sequential appearances of upper and lower yielding points and ultimate strength. Tensile strength was determined by failure strength with elasticity or little plasticity, and the upper yielding point in the high-rate region and by the ultimate strength in the low-rate region. The former strength was largely dependent on displacement rate, the latter rather independent. Strength tended to be saturated as displacement rate was raised to a very high-rate region, suggesting the presence of fast fracture strength peculiar to material and temperature. The time up to upper yielding point was roughly unproportional to the displacement rate, but tended to increase with increasing rate, probably due to the effect of time to spread cavitation zone. The fracture surface features was drastically changed with the appearance of rough areas of SCG as the rate was decreased; it was changed from a typical brittle fracture surface to that half covered by the rough area at 1260° C, and from that slightly covered to fully covered by the rough area at 1380° C. In the wake of SCG, a lot of holes from which long grains were pulled out and protruding grains from surface were observed, and stress re-increase after lower yielding point was attributed to increments of fracture resistance due to these pull-out contributions.

References

1. L. J. LINDBERG, in Proceedings of the 25th Automotive Technology Development Contractor's Coordination Meeting, October 1987 (Society of Automotive Engineers, 1987) p. 115.

2. R. K. GOVILLA, *J. Mater. Sci.* **23** (1988) 1141.
3. R. KOSSOWSKY, D. G. MILLER and E. S. DIAZ, *ibid.* **10** (1975) 983.
4. F. F. LANGE, E. S. DIAZ and C. A. ANDERSON, *Amer. Ceram. Soc. Bull.* **58** (1979) 845.
5. A. G. EVANS and S. M. WIEDERHORN, *J. Mater. Sci.* **9** (1974) 270.
6. F. F. LANGE, *J. Amer. Ceram. Soc.* **56** (1973) 518.
7. F. F. LANGE, *ibid.* **57** (1974) 84.
8. T. ISEKI, M. MORI and H. SUZUKI, *Yogyo-Kyokai-Shi* **86** (1978) 597.
9. R. K. GOVILLA, *J. Amer. Ceram. Soc.* **63** (1980) 319.
10. D. MUNZ, G. HIMSOLT and J. ESCHWEILER, *ibid.* **63** (1980) 341.
11. R. K. GOVILLA, *ibid.* **65** (1982) 15.
12. K. C. LIU and C. R. BRINKMAN, in Proceedings of the 23rd Automotive Technology Development Contractor's Coordination Meeting, October 1985 (Society of Automotive Engineers, 1985) p. 279.
13. S. G. SESHADRI and K. CHIA, *J. Amer. Ceram. Soc.* **70** (1987) C-242.
14. T. OHJI, *et al.*, *High Temp. Tech.* **5** (1987) 139.
15. T. OHJI, *et al.*, in Proceedings of the International Institute for the Science of Sintering Symposium, Tokyo, November 1987, edited by S. Somiya *et al.* (Elsevier, London, 1988) p. 1022.
16. A. G. EVANS and W. BLUMENTHAL, in "Fracture Mechanics of Ceramics", Vol. 6, edited by R. C. Bradt *et al.* (Plenum, New York, 1983) p. 423.
17. C. H. HSUEH and A. G. EVANS, *Acta Metall.* **29** (1981) 1907.
18. T. OHJI, *et al.*, *J. Ceram. Soc. Japan*, **98** (1990) March.
19. G. G. TRANTINA, *J. Amer. Ceram. Soc.* **62** (1979) 377.
20. Y. YAMAUCHI, *et al.*, *Nippon Seramikkusu Kyokai Gakujutsu Ronbunshi* **96** (1988) 885.
21. N. MURAYAMA, Government Industrial Research Institute, Hirate-cho, Kita-ku, Nagoya 462, Japan.
22. G. D. QUINN, F. I. BARATTA and J. A. CONWAY, Army Materials and Mechanics Research Centre 85-21 (1985).
23. Japanese Industrial Standard JIS R 1604 (Japan Standard Association, 1986).
24. R. K. GOVILLA, *J. Mater. Sci.* **14** (1979) 1095.
25. J. J. MECHOLSKY and S. W. FREIMAN, in "Fracture Mechanics Applied to Brittle Materials", ASTM STP 678 (American Society for Testing and Materials, 1979) p. 136.
26. T. OHJI, *et al.*, in Proceedings of the 30th Japanese Congress on Material Research, Kyoto, September 1986 (Society of Material Science, Japan, 1987) p. 201.
27. A. TSUGE, K. NISHIDA and M. KOMATSU, *J. Amer. Ceram. Soc.* **58** (1975) 323.
28. G. WOTTING and G. ZIEGLER, in Proceedings of the 1st International Symposium on Ceramic Components for Engine, Hakone, October 1983, edited by S. Somiya, E. Kanai and K. Ando (KTK/Reidal, Tokyo, 1984) p. 412.

Received 28 February
and accepted 30 August 1989